doi: 10.18323/2782-4039-2025-3-73-5

Special aspects of microstructure formation in Cu–Cr–Zr–Y bronze under low-temperature friction stir processing

Ivan S. Nikitin*[1], PhD (Engineering), junior researcher
of the Laboratory of Mechanical Properties of Nanostructured Materials and Superalloys
Aleksandr A. Kalinenko[2], PhD (Physics and Mathematics), junior researcher
of the Laboratory of Mechanical Properties of Nanostructured Materials and Superalloys
Sergey S. Malopheyev[3], PhD (Engineering), senior researcher of the Laboratory
of Mechanical Properties of Nanostructured Materials and Superalloys
Sergey Yu. Mironov[4], Doctor of Sciences (Physics and Mathematics), leading researcher
of the Laboratory of Mechanical Properties of Nanostructured Materials and Superalloys
Anna I. Bodyakova[5], PhD (Physics and Mathematics), researcher
of the Laboratory of Mechanical Properties of Nanostructured Materials and Superalloys
Belgorod State University, Belgorod (Russia)

***E-mail:** nikitin_i@bsuedu.ru

[1]ORCID: https://orcid.org/0000-0002-5417-9857
[2]ORCID: https://orcid.org/0000-0001-7534-0542
[3]ORCID: https://orcid.org/0000-0001-9145-3723
[4]ORCID: https://orcid.org/0000-0003-2202-1518
[5]ORCID: https://orcid.org/0000-0002-9378-0338

Received 15.07.2025 *Revised 26.08.2025* *Accepted 09.09.2025*

Abstract: The use of friction stir processing (FSP) to modify the physical and mechanical properties of age-hardenable low-alloyed bronzes is a promising and at the same time complex task due to the wide temperature range of its implementation. The difficulty is that friction stir processing of bronzes can result in the formation of fundamentally different types of microstructures with a wide range of grain sizes and various combinations of types of strengthening phases and their various morphologies. Moreover, options are possible when friction stir processing leads to degradation of properties of bronzes. A favorable combination of properties can be achieved by low-temperature friction stir processing. In this work, the main microstructural changes in promising Cu–Cr–Zr–Y bronze were analyzed during low-temperature friction stir processing with a tool rotation speed of 1000 rpm and a feed rate of 25 mm/min (ensuring a temperature in the stir zone of ≈350 °C). Scanning electron microscopy and EBSD analysis revealed the mechanisms of formation of an ultrafine-grained structure with predominantly high-angle boundaries, as well as the development of two types of simple shear crystallographic textures. It is shown that the Cu_x(Y,Zr) phase observed in the initial structure can undergo mechanical destruction or retain its geometric parameters depending on its initial morphology and location. It is shown for the first time that excess Cr particles (the equilibrium fraction at the heating temperature for quenching) may not be destroyed, but plastically deformed with a strong change in their morphology. During friction stir processing of the bronze under study, particles of a new Y-containing phase are released. The paper considered the relationship of the distribution of microhardness and electrical conductivity and the observed changes in the microstructure of a new promising material.

Keywords: friction stir processing; low-alloyed bronzes; recrystallization; secondary phases; electrical conductivity.

Acknowledgments: The study was supported by grant No. 24-29-00628 from the Russian Science Foundation (https://rscf.ru/project/24-29-00628/) using the equipment of the Common Use Center “Technology and materials of BSU”.

The paper was written on the reports of the participants of the XII International School of Physical Materials Science (SPM-2025), Togliatti, September 15–19, 2025.

For citation: Nikitin I.S., Kalinenko A.A., Malopheyev S.S., Mironov S.Yu., Bodyakova A.I. Special aspects of microstructure formation in Cu–Cr–Zr–Y bronze under low-temperature friction stir processing. *Frontier Materials & Technologies*, 2025, no. 3, pp. 67–80. DOI: 10.18323/2782-4039-2025-3-73-5.

INTRODUCTION

Friction stir processing (FSP) is one of the methods for increasing the strength characteristics of metallic materials by modifying the microstructure mainly due to grain refinement during dynamic recrystallization processes. Optimization of the FSP parameters of single-phase alloys aims to achieve a combination of two main characteristics: (1) to obtain a defect-free region and (2) to achieve grain refinement. The greatest difficulties arise with respect to alloys strengthened by particles of second phases, in particular by low-alloyed bronzes. For bronzes, defect-free processing zones can be obtained in a relatively wide temperature range (0.27–0.77 T_{melt}) [1–3], i.e. the process of friction stir processing can occur at various combinations of temperatures and deformation values. In this case, the process temperature will control the precipitation/dissolution and coarsening of particles of strengthening phases, as well as the size of dynamically recrystallized grains. In the works [2; 4], it is shown that a favorable combination of mechanical properties and electrical conductivity of Cu–Cr–Zr bronzes is achieved under the condition of carrying out the friction stir processing at temperatures near 0.27–0.40 T_{melt}, which is close to the temperatures of artificial aging of bronzes [5–7]. Thus, a favorable combination of bronze properties can be obtained after friction stir processing at fairly low temperatures limiting the size of recrystallized grains and ensuring the precipitation or stability (within acceptable limits) of strengthening particles. Considering the rather narrow range of FSP temperatures (0.27–0.40 T_{melt}), at which favorable combinations of physical and mechanical properties are achievable, it is worth mentioning that, in addition to the FSP parameters, the second equally important factor is the initial state of the bronze microstructure. The possibility of refining Cu–Cr–Zr bronze grains to a range of ≈160 nm approaching the nanoscale was demonstrated in [8], while the formation of ultrafine grains of ≈300 nm was demonstrated in [4]. In the first case, quenched plates were used as the processed material [8], while in the second case, the alloy was aged to maximum strength [4]. In both studies, an increase in the hardness and strength of the alloys was observed; however, the effect of friction stir processing on the electrical conductivity was significantly different. Friction stir processing of quenched bronze increased the electrical conductivity from 34 to 38–50 % IACS [8]. This increase is relatively small compared to the effect of aging. Probably, in this case, the process temperature was lower than the temperatures of intense decomposition of the solid solution (the temperature was not measured). Friction stir processing of aged bronze led to a slight decrease in electrical conductivity from 80 to 70–74 % IACS due to partial dissolution of Cr particles and an increase in its content in the matrix [4]. As a result, the most promising idea is to conduct low-temperature friction stir processing of quenched bronze, which in the long term can eliminate the procedure of subsequent aging aimed at the formation of hardening phases.

Low-alloyed bronzes of the Cu–Cr–Zr system are used in a wide range of applications, for example, in the manufacture of electrodes for contact welding, contact wires for railways, crystallizers for continuous casting of steel, liners in combustion chambers of rocket engines, blanket modules of thermonuclear reactors. A wide variety of applications allows believing that solid-phase FSP technology is promising in terms of modifying the structure, as well as the physical and mechanical characteristics of a number of critical parts.

Bronzes of the Cu–Cr–Zr–Y system are a new material; little research has been conducted on them. Therefore, it is very difficult to predict the behavior of this material during friction stir processing: to estimate the kinetics of grain refinement, phase composition, response of physical and mechanical characteristics to the evolution of the microstructure, which justifies significant scientific and practical interest in this work. Additional alloying of the Cu–Cr–Zr system bronze with Y was used for refining [9] and additional dispersion strengthening – in the Cu–Y system at temperatures below ≈900 °C, the solubility of Y in the matrix decreases [10]. It means that in quenched bronze with the addition of Y, upon subsequent heating to temperatures below ≈900 °C (during aging or heating during friction stir processing), the precipitation of strengthening phases is possible.

The aim of this work is to identify the main patterns of microstructure formation in bronze of the Cu–Cr–Zr–Y system under low-temperature friction stir processing and to assess the influence of microstructural changes on hardness and electrical conductivity.

METHODS

The material for the study was Cu–0.9%Cr–0.17%Zr–0.05%Y (wt. %) bronze. The initial state was obtained by forging a cast billet at temperatures of 850–1000 °C in air and cooling followed by heating to 920 °C (holding for 1 h) and cooling in water. After that, the billet was cut into 3 mm thick plates. Friction stir processing was carried out using a hemispherical tool with a pin diameter of 5 mm and flat shoulders with a diameter of 12 mm made of WC+Co hard alloy.

The FSP experiments were carried out on an AccuStir 1004 installation (USA) at a tool rotation speed of 1000 rpm and a feed rate of 25 mm/min with a tool tilt of ≈2.5° and a penetration depth of 2.8 mm. The selected parameters are determined by the results of temperature measurements in a number of experiments on the friction stir processing at a rotation speed of 1000 rpm and varying feed rates (the mode with the lowest temperature and without external defects was selected). A sheet of 09G2S steel with a thickness of 4 mm was used as a substrate (a material under the bronze sheet).

Temperatures (thermal cycle) at the edge of the stir zone (SZ) were measured using a FLUKE 54 II B thermometer (USA) using chromel-alumel thermocouples. The temperature was measured at the middle of the sheet thickness. The measured maximum temperature of the friction stir processing did not exceed 350 °C.

Macro- and microstructure were studied on a transverse section after vibration polishing on a Buehler VibroMet 2 installation (USA) in an OP-U suspension for 24 h.

The macrostructure was analyzed after etching the polished sample in a mixture of 100 ml of 30 % H_2O_2 and 5 ml of H_2SO_4 using an Olympus GX51 optical microscope (Japan). The microstructure (in the Z-contrast mode) was studied using a Quanta 600 FEG scanning electron microscope (SEM) (USA) equipped with an attachment for energy-dispersive analysis of the composition and an EBSD attachment (an attachment for analyzing electron backscatter diffraction patterns).

In this work, two areas of the sample were studied: (1) the top of the SZ – at a distance of 50 μm from the surface of the processed zone and (2) the center of the SZ. For each of the states, EBSD maps of 50×50 μm in size with a scanning step of 0.1 μm were obtained. The data were processed and analyzed using TSL OIM Analysis 8 software. For texture analysis, EBSD maps were cleaned by removing all points with a CI (confidence index) of less than 0.1. To estimate the average grain size and grain misorientations, cleaning was performed using the standard "grain dilation" function with a minimum grain misorientation threshold of 15° and a minimum grain size of 3 pixels.

Vickers microhardness profiles were obtained in the middle of the FSP zone thickness using a Wolpert 402MVD microhardness tester (Netherlands) with a load of 100 g, a holding time of 10 s, and a measurement step of 0.25 mm.

The IACS relative conductivity (according to the International Annealed Copper Standard) was estimated as a percentage of the annealed copper conductivity of 58.1 mS/m at 20 °C:

$$\text{IACS} = \frac{100\,\% \times \text{Bronze electrical conductivity}}{58.1}.$$

The relative conductivity profiles were obtained by the eddy current method using a Constant K-6 installation (RF) by taking measurements with a step of 1 mm from the surface of the plate perpendicular to the FSP direction after grinding on 1000 grit sandpaper.

Thermodynamic modeling of the equilibrium phase composition was carried out using the Thermo-Calc software package using the TCHEA4: High Entropy alloys v. 4.2 database.

RESULTS

Microstructure in the initial state

The microstructure of bronze in the initial state is represented by large grains with an average size of 64±35 μm (excluding twin boundaries), within which multiple annealing twins were observed (Fig. 1).

Most of the grain boundaries were decorated with a second phase interlayer, which stood out strongly against the matrix background in the Z-contrast mode in the form of light contrasting areas (Fig. 1 a). The composition assessment showed that these areas are enriched in Cu, Zr and Y with a total content of (Y+Zr) in the range of 8–15 at. %, as shown in Fig. 1 c. The detected phase can be designated by the formula Cu_x(Y,Zr), where x varies from 5.6 to 9.7. The study at high magnifications (Fig. 1 b) showed that the light areas have an uneven contrast, which is associated with the heterogeneity of the Zr distribution (Fig. 1 b, d). In addition to the grain boundary arrangement, a (Y+Zr)-rich phase in the form of spherical inclusions with sizes from 4 to 18 μm (Fig. 1 c) was observed in the grain body. In some cases, the inclusions were located on black particles.

The microstructure also contained multiple homogeneously distributed particles with an average size of 1.02±0.78 μm with a black contrast, which were enriched with 78–98 at. % of Cr (Fig. 1).

Macrostructure after friction stir processing

The macrostructure of the sample after the friction stir processing is represented by different zones, which include the stir zone (SZ), the thermo-mechanically affected zone (TMAZ), and the base material zone, which is schematically shown in Fig. 2. Fig. 2 a shows the location of the stirring tip relative to the observed zones showing that the stir zone is not limited by the pin size, but expands towards the edges of the tool shoulders. Along the entire periphery of the stir zone, there is a TMAZ (Fig. 2 b, d) represented by fibers of elongated grains, followed by the main material zone with large grains.

Three types of inclusions are observed in all macrostructural zones of the treated area (Fig. 2 e, f, g): (1) gray spherical particles, (2) black areas of irregular morphology and (3) black spherical particles with internal inclusions and a contrast close to the matrix.

Microstructure and crystallographic texture after friction stir processing

The microstructure of bronze after FSP is represented by submicron grains with a fraction of high-angle boundaries of about 0.85 both at the top and in the center of the SZ – Fig. 3, 4 and Table 1. According to the data obtained by SEM, the average grain size in both areas of the SZ was ≈0.28 μm, while according to the EBSD results – ≈0.35–0.40 μm. Comparison of the size distribution shows that the measured values fall into the same size range from 0.15 to 0.8–1.0 μm and differ only in the intensities of each of the size groups, which is also reflected in the overlap of the average sizes taking into account the standard deviation of the value (Table 1). It means that the presented data are representative and reliable. The grains have a deviation from equiaxiality, as evidenced by the shape factor (SF) value equal to 1.99 for the top and 1.82 for the center of the SZ. In general, the friction stir processing leads to a decrease in the average grain size by 200 times.

The obtained experimental distributions of the misorientation angles of the top and center of the SZ are qualitatively similar to each other (Fig. 5). The distribution is characterized by the presence of two main maxima at small (≈2.5°) and large (≈45°) angles of misorientations with an intensity of up to 4 %. The experimental distribution of misorientation angles, random distribution and texture-induced distribution show the presence of a maximum in the angle range near ≈45°.

It is believed that the deformation scheme under FSW/FSP is close to the simple shear scheme [15], in this case, the shear surface can be the surface of the hemispherical

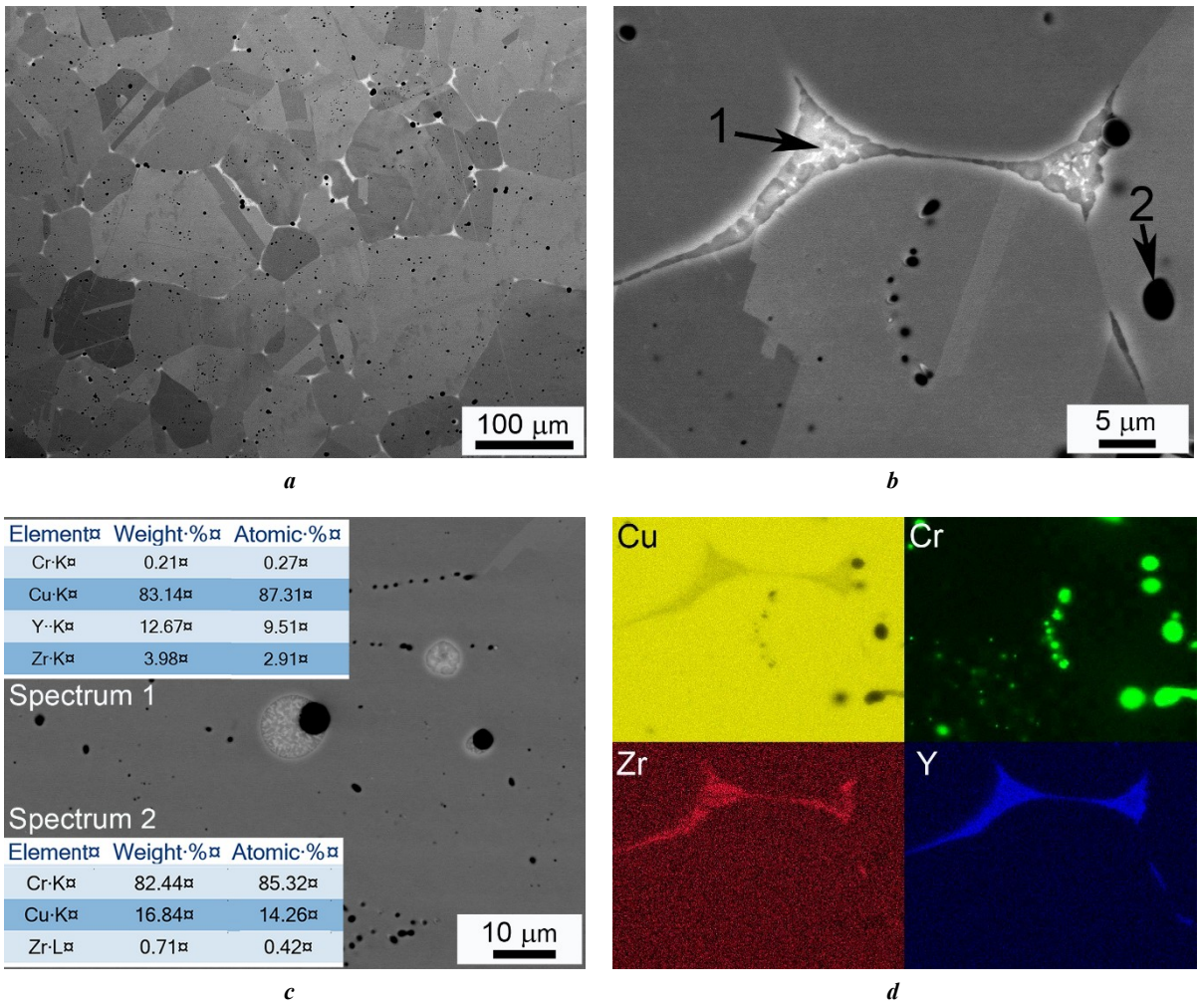

Fig. 1. *Microstructure of bronze in initial state:*
a *– general view at ×500 magnification;* ***b*** *– grain boundary phase and particles in the grain body at ×6000 magnification;* ***c*** *– (Y+Zr)-enriched inclusions in the grain body and chemical compositions of the grain boundary phase (spectrum 1) and particles in the grain body (spectrum 2);* ***d*** *– distribution of elements in Fig. 1 b between phases*
Рис. 1. *Микроструктура бронзы в исходном состоянии:*
a *– общий вид при увеличении ×500;* ***b*** *– зернограничная фаза и частицы в теле зерна при увеличении ×6000;* ***c*** *– (Y+Zr)-обогащенные включения в теле зерна и химические составы зернограничной фазы (спектр 1) и частицы в теле зерна (спектр 2);* ***d*** *– распределение элементов на рис. 1 b между фазами*

pin or the lower surface of the shoulders, while the shear direction is tangential to the tool surface. Thus, the shear geometry varies greatly in different parts of the SZ. To reveal the crystallographic texture in the sample, it is necessary to rotate the EBSD map. Experimental and corrected maps with rotation angles relative to different directions are shown in Fig. 6. Pole figure analysis showed that the entire SZ exhibits the formation of a combination of axial <110> and limited $B/\bar{B}$ {112}<110> simple shear textures.

Analysis of secondary phases revealed the following features. Both at the top and in the center of the SZ after FSP, contrasting spherical inclusions were observed, which were previously observed in the initial state (Fig. 7). It is worth noting that grain boundary phases were not observed. For visual comparison, the micrographs in Fig. 1 a and Fig. 7 are presented at the same magnification (×500). The main differences between the top and center of the SZ are that at the top of the stir zone, contrasting white banded structures elongated along the direction of rotation were observed.

During the initial analysis of the microstructure by the SEM method in the Z-contrast mode at high magnifications, contrasting black bands were observed in the studied zones of the sample (Fig. 8 a, b), the direction of which coincided with the direction of tool rotation. Such bands could have unclear outlines and bend repeatedly. Analysis of the distribution maps of the alloy components (Fig. 8 c, d, e, f, g, h) revealed that these are strongly deformed particles "smeared" between the matrix layers, enriched with Cr. After FSP, Cr particles had a wide variety of morphologies, ranging from large spherical particles to repeatedly bending plates and particles of variable shape, which differed much from the morphology of Cr particles of predominantly spherical shape in the initial state (Fig. 1).

In the microstructure of the studied zones after FSP, a few particles of a new phase enriched in Y were detected

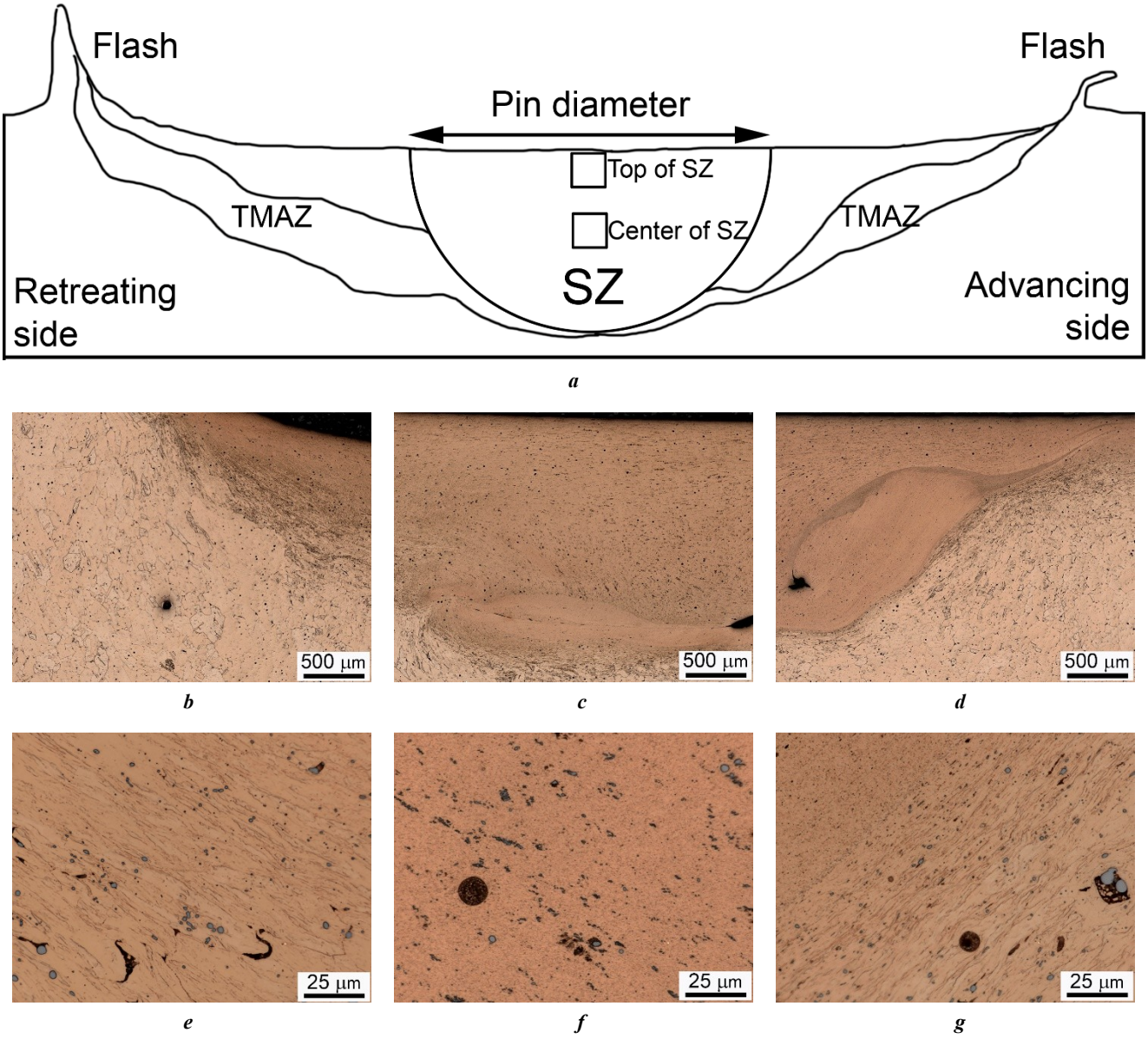

Fig. 2. *Schematic arrangement of macrostructural zones of the studied sample and images of individual zones (optical microscopy):* ***a*** *– diagram of macrostructural zones;* ***b, e*** *– thermo-mechanically affected zones (TMAZ) on the material retreating side at magnifications of ×5 and ×100;* ***c, f*** *– stir zones (SZ) at magnifications of ×5 and ×100;* ***d, g*** *– TMAZ on the material advancing side at magnifications of ×5 and ×100*

Рис. 2. *Схема расположения макроструктурных зон исследуемого образца и изображения отдельных зон (оптическая микроскопия):* ***a*** *– схема макроструктурных зон;* ***b, e*** *– зоны термомеханического влияния (TMAZ) со стороны отвода материала при увеличении ×5 и ×100;* ***c, f*** *– зоны перемешивания (SZ) при увеличении ×5 и ×100;* ***d, g*** *– TMAZ со стороны набегания материала при увеличении ×5 и ×100*

(Fig. 8 a, b, e, f), while traces of the presence of Zr (Fig. 8 a, b, g, h) were not observed in these particles.

Microhardness and electrical conductivity after friction stir processing

The treated zone was characterized by a non-uniform distribution of microhardness and electrical conductivity (Fig. 9) with a smooth increase in the characteristics in the direction from the material retreating side (RS) to the material advancing side (AS) and their sharp decrease at the boundary of the SZ at the stirring tip interface. Almost the entire width of the zone of changed microhardness and electrical conductivity corresponds to the diameter of the tool shoulders, which indicates that most of the heat is concentrated under the tool and the heat-affected zone practically does not extend beyond its boundaries.

Extreme values of microhardness and electrical conductivity were observed at the edge of the SZ with AS and reached ≈240 HV and ≈76 % IACS. In the center of the SZ, the indicators were lower and corresponded to ≈167 HV and ≈72 % IACS, which is 2.9 and 1.6 times higher than the values in the initial state (≈58 HV and ≈45 % IACS).

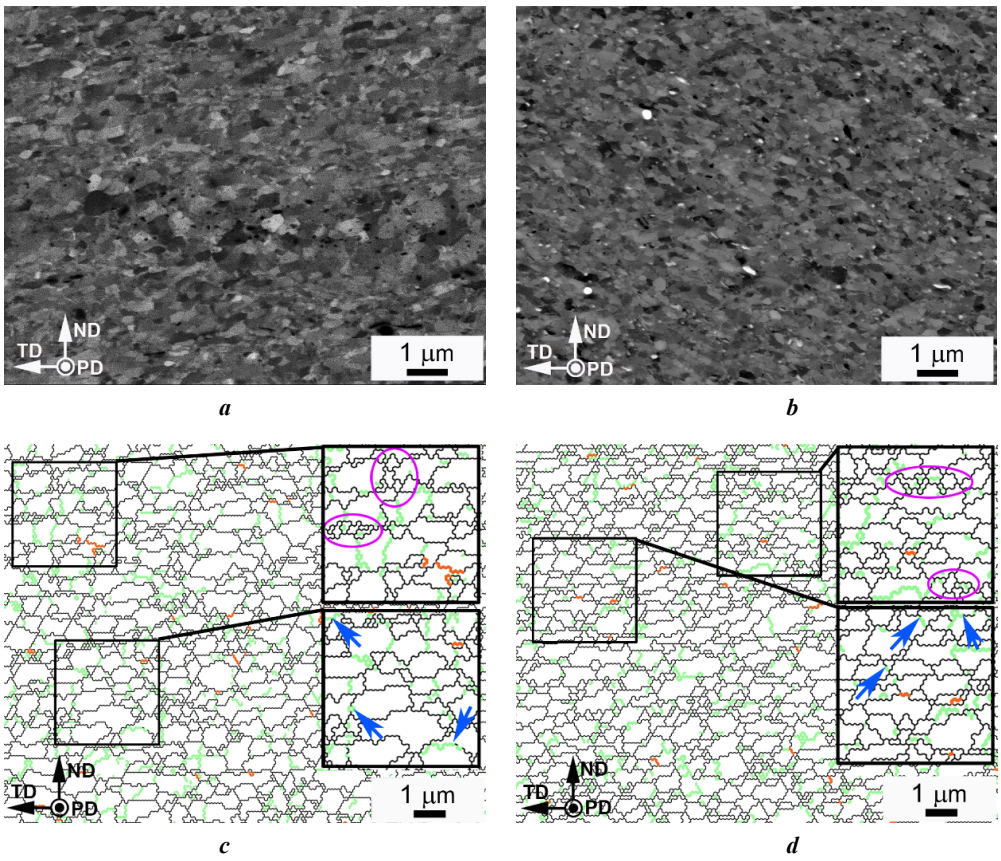

Fig. 3. *Microstructure after friction stir processing at the top and center of the stir zone (SZ): SEM micrographs of the top (**a**) and center of the SZ (**b**); EBSD maps of the top (**c**) and center of the SZ (**d**).*
On the maps, low-angle misorientation (2–15°) boundaries are shown in green, high-angle misorientation (15–63°) boundaries are shown in black, and 60°<111> twin boundaries are shown in red.
*Blue arrows (**c, d**) highlight low-angle boundaries that progress in misorientation to high-angle boundaries.*
Groups of small grains at the boundaries between relatively large grains are outlined in purple.
The PD, ND, and TD designations correspond to the processing direction, normal direction, and transverse direction
Рис. 3. *Микроструктура после обработки трением с перемешиванием вверху и в центре зоны перемешивания (ЗП): микрофотографии РЭМ верха (**a**) и центра ЗП (**b**); EBSD-карты верха (**c**) и центра ЗП (**d**).*
На картах границы малоугловой разориентировки (2–15°) обозначены зеленым цветом, границы большеугловой разориентировки (15–63°) обозначены черным цветом, двойниковые границы 60°<111> обозначены красным цветом.
*Синими стрелками (**c, d**) выделены малоугловые границы, набирающие свою разориентировку до большеугловых границ.*
Фиолетовым цветом обведены группы мелких зерен на границах между относительно крупными зернами.
Обозначения PD, ND и TD соответствуют направлению обработки, направлению нормали и поперечному направлению

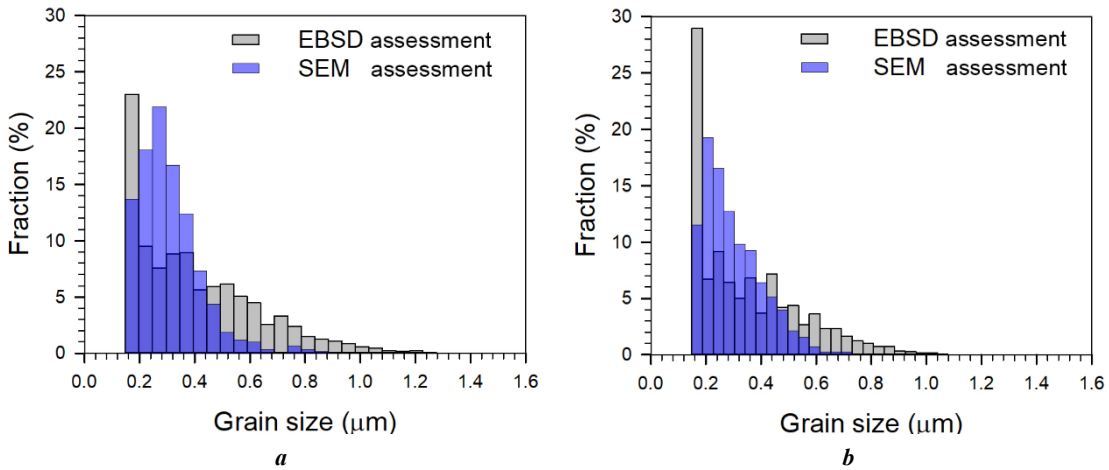

Fig. 4. *Grain size distribution after friction stir processing at the top (**a**) and center (**b**) of the stir zone*
Рис. 4. *Размерное распределение зерен после обработки трением с перемешиванием вверху (**a**) и в центре (**b**) зоны перемешивания*

Table 1. *Microstructure parameters after friction stir processing*
Таблица 1. *Параметры микроструктуры после обработки трением с перемешиванием*

Stir zone area	d_{av} (EBSD) (μm)	d_{av} (SEM) (μm)	SF (SEM)	F_{HAB}/F_{LAB}	θ_{av} (deg)
Top of the stir zone	0.40±0.23	0.28±0.11	1.99	0.86/0.14	36.4
Center of the stir zone	0.35±0.19	0.28±0.11	1.82	0.84/0.16	36.0

Note. d_{av} *is average grain size; SF is grain shape factor as the ratio of the maximum size to the minimum one;* F_{HAB} *and* F_{LAB} *are fractions of high-angle and low-angle boundaries;* θ_{av} *is average angle of misorientation of boundaries.*

Примечание. d_{av} *– средний размер зерна; SF – коэффициент формы зерна в виде отношения максимального размера к минимальному;* F_{HAB} *и* F_{LAB} *– доли большеугловых и малоугловых границ;* θ_{av} *is средний угол разориентировки границ.*

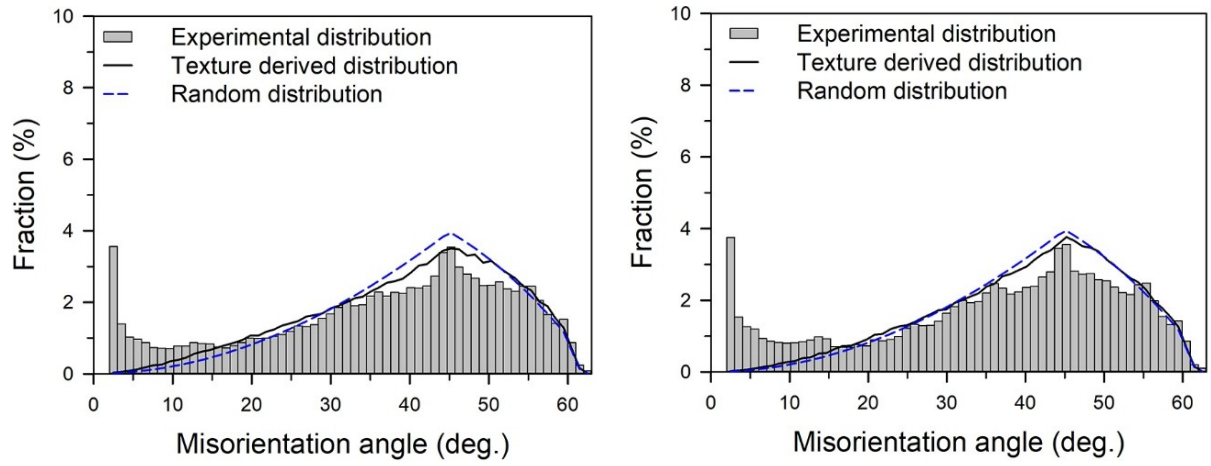

Fig. 5. *Distribution of misorientation angles after friction stir processing at the top (**a**) and in the center (**b**) of the stir zone*
Рис. 5. *Распределение углов разориентировки после обработки трением с перемешиванием вверху (**a**) и в центре (**b**) зоны перемешивания*

DISCUSSION

Characteristics of phase composition in the initial state

A phase containing 8–15 at. % of (Y+Zr) designated Cu_x(Y,Zr) with an x parameter varying from 5.6 to 9.7 was detected in the microstructure of bronze after quenching. According to sources [10; 11], it can be classified as a Cu_6Y/Cu_7Y-type phase with a hexagonal crystal lattice of the P6/mmm type. This phase can dissolve 12–16 at. % of Y, which is consistent with the total (Y+Zr) content reported in the study. The heterogeneity of the Zr distribution within the grain boundary phase shown in Fig. 1 may be caused by the dendritic heterogeneity in the phase composition or by the presence of multiple phases within the structure of Y- and Zr-rich regions. A similar phenomenon was illustrated in [12] using the example of Cu–0.5Y–(0.05–0.1)Zr alloys, in which particles consisting of metastable Cu_5Y+Cu_5Zr phases are formed during casting. Considering the fact that the average (Y+Zr) contents determined in the study are also similar to the compositions of the Cu_5Y+Cu_5Zr phases [12], we cannot exclude the possibility that a metastable phase is observed in the case under consideration.

The second phase observed in the microstructure consists predominantly of Cr. Considering the large size of the particles and the fact that they are observed in the quenched state, they are likely equilibrium particles of the body-centered cubic lattice of Cr [13], which did not dissolve during heating and holding during quenching. The presence of these particles is in good agreement with the equilibrium diagram of Cu–Cr state at a heating temperature for quenching of 920 °C [14].

Characteristics of grain structure and texture formation after FSP

An ultrafine-grained structure with an average grain size of ≈0.3 μm forms in the upper and central parts of the SZ. To determine the dominant recrystallization mechanism responsible for microstructure formation, we consider the distribution of misorientation angles of the formed grains in different regions of the stir zone (Fig. 5). Comparison with the results of other studies on FSW/FSP of bronzes of the Cu–Cr–Zr system [2–4] indicates that the low fraction of 2–3° of boundaries is associated with a decrease in the process temperature: at a temperature of 790 °C, the relative fraction of such boundaries is ≈18 % [3], at 440 °C,

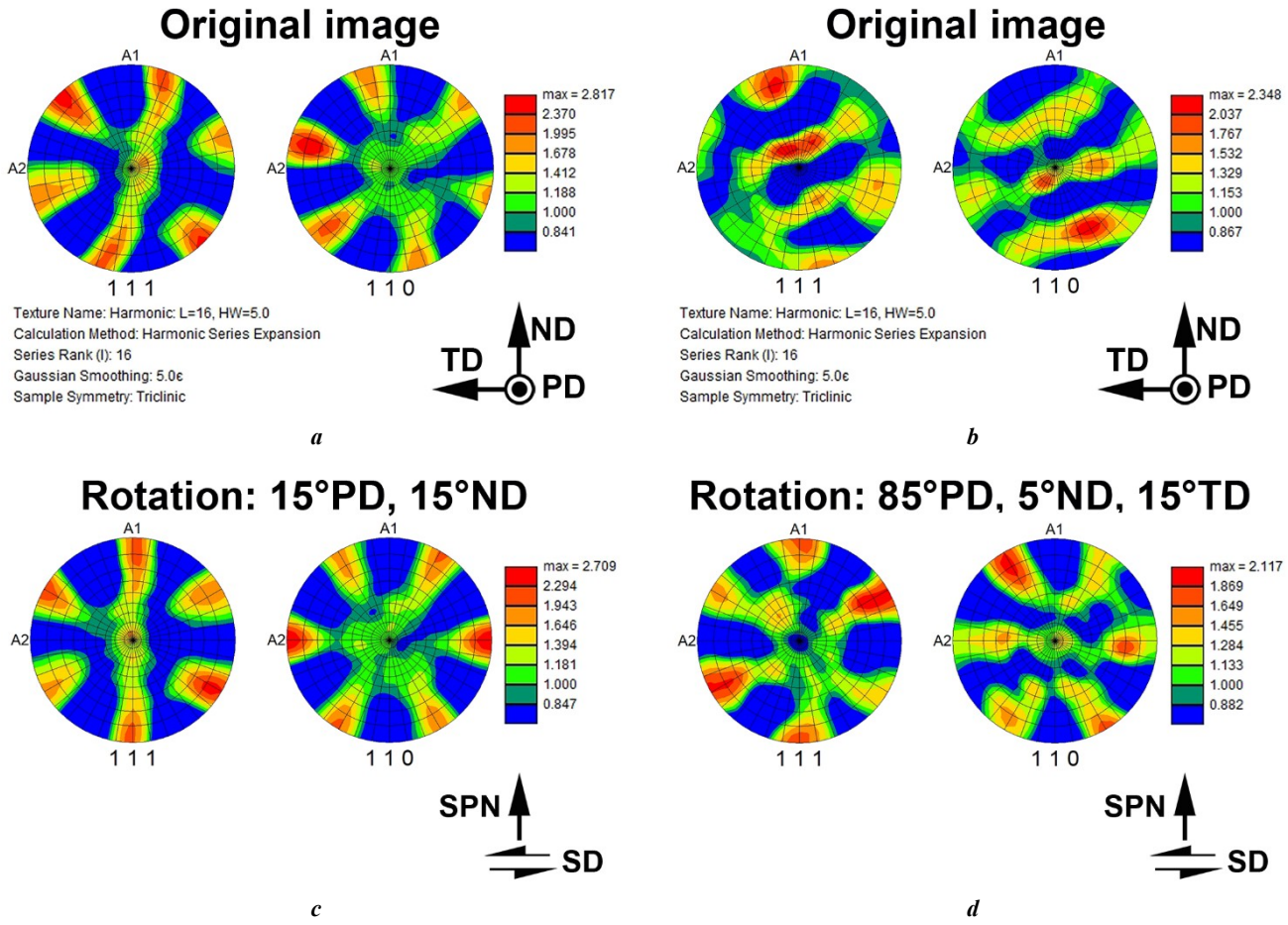

Fig. 6. *Experimental (**a, b**) and corrected (rotated) pole figures (**c, d**) of {111} and {110} obtained after friction stir processing at the top (**a, c**) and center (**b, d**) of the stir zone, illustrating the formed texture. The PD, ND, and TD designations (**a, b**) correspond to the processing direction, normal direction, and transverse direction. The SD and SPN designations (**c, d**) correspond to the shear direction and the shear plane normal direction. The rotation angles of the experimental pole figures are indicated at the top of the figure.*

Рис. 6. *Экспериментальные (**a, b**) и скорректированные (развернутые) полюсные фигуры (**c, d**) {111} и {110}, полученные после обработки трением с перемешиванием вверху (**a, c**) и в центре (**b, d**) зоны перемешивания, иллюстрирующие сформировавшуюся текстуру. Обозначения PD, ND и TD (**a, b**) соответствуют направлению обработки, направлению нормали и поперечному направлению. Обозначения SD и SPN (**c, d**) соответствуют направлению сдвига и направлению нормали к плоскости сдвига. В верхней части рисунка указаны углы разворота экспериментальных полюсных фигур*

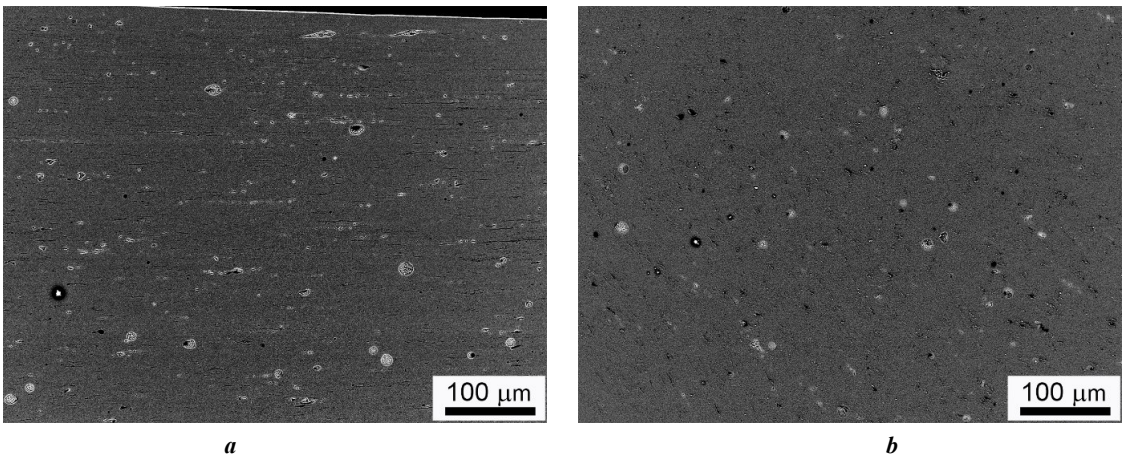

Fig. 7. *Microstructure after friction stir processing at the top (**a**) and center (**b**) of the stir zone at ×500 magnification*

Рис. 7. *Микроструктура после обработки трением с перемешиванием вверху (**a**) и в центре (**b**) зоны перемешивания при увеличении ×500*

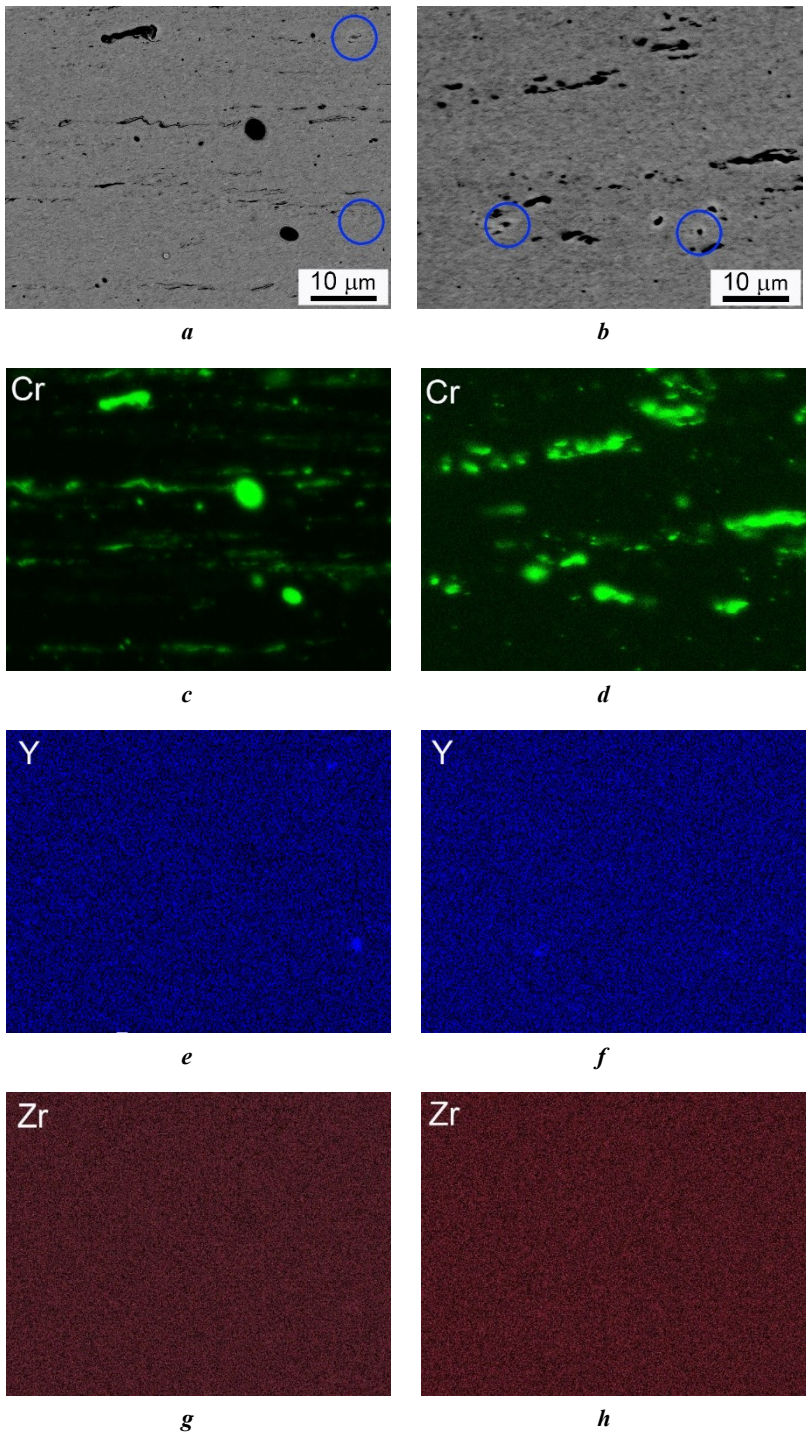

Fig. 8. *Secondary phase particles (**a, b**) in combination with the distribution of Cr (**c, d**), Y (**e, f**) and Zr (**g, h**) between the phases after friction stir processing at the top (**a, c, e, g**) and in the center (**b, d, f, h**) of the stir zone*
Рис. 8. *Частицы вторичных фаз (**a, b**) в сочетании с распределением Cr (**c, d**), Y (**e, f**) и Zr (**g, h**) между фазами после обработки трением с перемешиванием вверху (**a, c, e, g**) и в центре (**b, d, f, h**) зоны перемешивания*

a decrease to ≈9 % [2] is observed, and at a temperature of 240 °C, a decrease to ≈6 % is observed [4]. This is in good agreement with the results presented in Fig. 4.

It is worth noting that the distribution of angle misorientations (Fig. 5) does not show a clearly defined peak of 60°<111> twin boundaries – these boundaries are shown by red lines in Fig. 3. In the initial state, a large number of annealing twin boundaries are observed (Fig. 1 a). As a result, the low fraction of 60°<111> boundaries after FSP can be associated with the low rate of metadynamic recrystallization during plate cooling after processing. The presence of a bimodal distribution (with peaks in the low- and high-angle regions) in Fig. 5 may indicate the dominance of continuous dynamic recrystallization processes. In addition, Fig. 3 c, d show segments of low-angle boundaries that gain their misorientation up to high-angle boundaries, which is also a direct marker of continuous recrystallization. At the same time, Fig. 3 c, d show

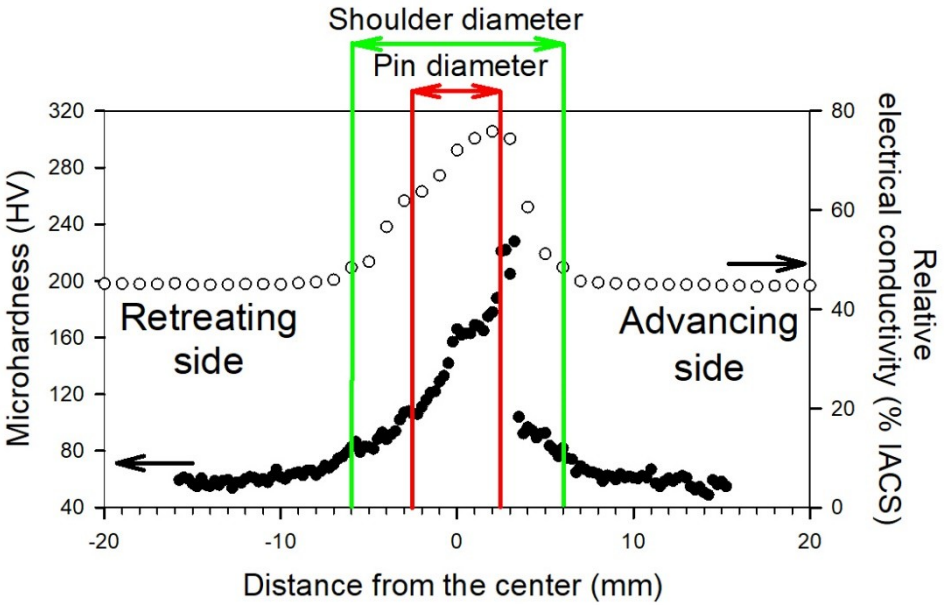

Fig. 9. *Distribution of microhardness and relative electrical conductivity in the zone of friction stir processing*
Рис. 9. *Распределение микротвердости и относительной электропроводности в зоне обработки трением с перемешиванием*

configurations of larger grains surrounded by groups of grains an order of magnitude smaller, which may indicate the presence of discontinuous dynamic recrystallization processes. It is likely that two dynamic recrystallization mechanisms compete during the FSP process. However, taking into account the low process temperature, the contribution of the continuous recrystallization mechanism can be considered predominant.

Comparison of the experimental misorientation spectrum with a random distribution (Fig. 5) and a distribution determined by crystallographic texture showed that the texture derived distribution has a smaller discrepancy, indicating that in this case, the emerging angle distribution may be determined by the developing crystallographic texture.

Based on the different rotation angles of the pole figures required to reveal texture at the top and center of the SZ, it is possible to say about the influence of different parts of the stirring tool on texture formation. Thus, small rotation angles were required near the SZ surface, indicating a greater influence of the flat tool shoulders during texture formation than the pin. At the center of the SZ, significant rotation angles were required, indicating a strong influence of the hemispherical pin on the crystallographic texture formation. However, the resulting distributions of misorientation angles (Fig. 5) and crystallographic textures (Fig. 6) in the zones under consideration are qualitatively and quantitatively similar, i.e., the mechanism of the misorientation distribution formation must be the same.

Returning to the relationship between grain misorientation angles near 45° and texture, the CLS boundaries function was used to estimate the fraction of special grain boundaries. Thus, a total of ≈2.4 % of the Σ9 – 38.9°<110> and Σ11 – 50.5°<110> boundaries were observed in the structure, the direction of which coincided with the identified predominant texture directions. Moreover, a total of ≈2.4 % of the Σ7 – 38.2°<111> and Σ29a – 43.6°<100> boundaries were observed, the directions of which were not related to texture. It can be assumed that these boundaries form the observed peak, with some of the boundaries associated with the crystallographic texture.

Characteristics of secondary phase changes during FSP

As noted previously, after friction stir processing, spherical inclusions with a Z-contrast were observed in the microstructure, which were identical to $Cu_x(Y,Zr)$ inclusions observed in the initial state. Their size, however, remained unchanged compared to the initial size. It can be assumed that these inclusions are not deformed during FSP, and the deformed matrix, due to its greater plasticity, "flows" around them during deformation. At the same time, the $Cu_x(Y,Zr)$ phase located at the original grain boundaries before FSP is ground into smaller fragments, which are arranged in banded structures aligned with the direction of tool rotation. In this case, the phase is arranged as a flat obstacle located at the boundary, which cannot be overcome during copper matrix flow, causing its partial destruction and rotation of the remaining fragments. Thus, the initial morphology of this phase significantly influences its evolution during FSP.

As has been shown, FSP significantly changes the morphology of Cr particles. The presence of elongated, repeatedly bending, plate-like particles is worth noting individually. A similar effect was not observed after FSP at higher temperatures. The authors believe that this particle morphology is associated with the high strain during FSP,

which can reach true values of ≈35 units [16]. The following mechanism for the change in Cr particle morphology can be hypothesized: the formation of an ultrafine-grained matrix structure increases the material's ability to resist deformation, thereby increasing internal stresses in the material. The material is heated to a temperature of ≈350°, and this combination of thermomechanical conditions likely becomes sufficient for plastic flow of Cr between the matrix grain layers.

During FSP of the Cu–Cr–Zr–Y bronze under study, particles enriched in Y and free of Zr were observed, although in the initial state, there was a phase containing both elements. It is appropriate to consider this phenomenon from the point of view of the analysis of the equilibrium phase diagrams of Cu–Zr and Cu–Y. After treatment with a supersaturated solid solution, Y and Zr can be present in the supersaturated solid solution in accordance with the phase diagram [11; 17]. According to the Cu–Y diagram [11], the closest phase to a given Y content is Cu_7Y, which exists at temperatures below 871 °C, whereas according to Cu–Zr diagram [17], the closest phase to a given Zr content is Cu_9Zr_2, which exists at temperatures below 972 °C. One can assume that Zr-enriched phases will precipitate at higher temperatures (a difference of about 100 °C). According to differential scanning calorimetry data for quenched Cu–Cr–Zr alloy, the precipitation of the Zr-enriched phase occurs at temperatures of about 490 °C [18]. Considering the fact that additional severe plastic deformation in most cases lowers the precipitation temperature of the second phase [18; 19], in combination with the expected difference in the precipitation temperatures of phases with Zr and Y, we naturally observe the precipitation of a Y-enriched phase. Additional thermodynamic modeling of the equilibrium phase composition at temperatures of 350–1100 °C using the Thermo-Calc program predicts the existence of the Cu_5Zr (C15B crystal lattice) and Cu_7Y (P6/mmm crystal lattice) phases in this temperature range. The temperature range of the existence of Cu_5Zr is from 580 to 910 °C, while for the Cu_7Y phase it corresponds to temperatures from 350 to 837 °C. It is quite natural that after low-temperature FSP, we observe a Y-enriched phase and do not observe phases with Zr. Thus, it can be assumed that the phase observed after FSP is the equilibrium Cu_7Y phase.

The relationship between properties and the forming microstructure during FSP

Having analyzed the observed characteristics of the microstructure, one can identify the relationship between the microstructure evolution and the formation of the distribution of microhardness and electrical conductivity. It is assumed that the asymmetric nature of the distributions combined with the gravitation of extreme values of the quantities to the advancing side (AS), is associated with the uneven distribution of temperature and strain in the deformation zone, shown by the modeling results [20]. In particular, the temperature with AS can be higher than with the retreating side (RS). Considering the fact that we observe a simultaneous increase in microhardness and electrical conductivity, it can be assumed that this phenomenon is associated with both the refinement of the grain structure and the decomposition of the supersaturated solid solution. The refinement of the grain structure in the stir zone was illustrated in the work. With regard to the decomposition of the supersaturated solid solution, only the precipitation of Y-enriched particles was shown, the amount of which in the microstructure (according to Fig. 8) is small. The maximum electrical conductivity of the treated area reaches 76 % IACS, which is close to the values of aged Cu–Cr–Zr bronze [3], corresponding to the microstructural state after the decomposition (partial or complete) of the solid solution. The high electrical conductivity value indirectly indicates the occurrence of intensive decomposition of the supersaturated solid solution with the release of nanometer-sized Cr and Zr particles during the FSP process. It is likely that the SEM method used in this study is insufficient for the resolution of the nanoscale particles of secondary phases formed at such a low temperature.

CONCLUSIONS

In the work, the following patterns of microstructure formation in Cu–Cr–Zr–Y bronze were identified during low-temperature friction stir processing:

1) friction stir processing caused the grain structure refinement to an average grain size of ≈0.3 μm with predominantly high-angle boundaries and the formation of a combination of axial <110> and limited $B/\bar{B}$ {112}<110> simple shear textures;

2) friction stir processing led to a destruction of the $Cu_x(Y,Zr)$ phase located along the boundaries of the original grains, but did not destroy this phase with a spherical morphology. FSP altered the morphology of Cr particles due to their deformation and elongation in the direction of tool rotation. FSP was accompanied by the precipitation of a Y-enriched phase not observed in the initial state;

3) microstructural changes occurring during FSP led to an increase in the values of microhardness and electrical conductivity in comparison with the quenched state.

REFERENCES

1. Makarov A.V., Lezhnin N.V., Kotelnikov A.B., Vopneruk A.A., Korobov Yu.S., Valiullin A.I., Volkova E.G. Restoration of continuous casting machine mold copper plates made of Cr-Zr bronze using multi-pass friction stir lap welding. *Izvestiya. Non-Ferrous Metallurgy*, 2023, vol. 29, no. 6, pp. 66–83. DOI: 10.17073/0021-3438-2023-6-66-83.
2. Bodyakova A.I., Chistyukhina E.I., Tkachev M.S., Malofeev S.S., Kaibyshev R.O. Effect of Friction Stir Processing on the Structure and Properties of the Low-Doped Cu–Cr–Zr Alloy. *Physics of Metals and Metallography*, 2024, vol. 125, no. 11, pp. 1192–1200. DOI: 10.1134/S0031918X24601677.
3. Bodyakova A., Malopfeev S., Tkachev M., Chistyukhina E., Mironov S., Lezhnin N., Fu Y., Makarov A., Kaibyshev R. Effect of friction-stir processing and subsequent aging treatment on microstructure and service properties of Cu-Cr-Zr alloy. *Materials Characterization*, 2024, vol. 216, article number 114225. DOI: 10.1016/j.matchar.2024.114225.
4. Wang Y.D., Liu M., Yu B.H., Wu L.H., Xue P., Ni D.R., Ma Z.Y. Enhanced combination of mechanical properties

and electrical conductivity of a hard state Cu-Cr-Zr alloy via one-step friction stir processing. *Journal of Materials Processing Technology*, 2021, vol. 288, article number 116880. DOI: 10.1016/j.jmatprotec.2020.116880.
5. Khomskaya I.V., Zel'dovich V.I., Frolova N.Y., Abdullina D.N., Kheifets A.E. Investigation of Cu_5Zr particles precipitation in Cu-Zr and Cu-Cr-Zr alloys subjected to quenching and high strain rate deformation. *Letters on Materials*, 2019, vol. 9, no. 4, pp. 400–404. DOI: 10.22226/2410-3535-2019-4-400-404.
6. Ma Yuxia, Chen Huiqin, Li Hui, Dang Shue. Influence Mechanism of Ageing Parameters of Cu-Cr-Zr Alloy on Its Structure and Properties. *Materials*, 2022, vol. 15, no. 21, article number 7605. DOI: 10.3390/ma15217605.
7. Khomskaya I.V., Zel'dovich V.I., Abdullina D.N., Shorokhov E.V. The Effect of Chromium and Zirconium Alloying on the Structure and Properties of Submicrocrystalline Copper Alloys Obtained by Dynamic Channel-Angular Pressing. *Physics of Metals and Metallography*, 2024, vol. 125, no. 10, pp. 1156–1165. DOI: 10.1134/s0031918x24601434.
8. Li Yijun, Zhang Jinghua, Fu Ruidong, Wang Jungao, Lv Hongyan, Xing Haizhi. Synergistic improvement of strength and electrical conductivity in Cu–Cr–Zr alloys through prestrain-assisted friction stir processing. *Journal of Materials Research and Technology*, 2023, vol. 27, pp. 564–573. DOI: 10.1016/j.jmrt.2023.09.262.
9. Li Hai-hong, Sun Xue-qin, Zhang Shang-zhou, Zhao Qin-yi, Wang Guang-zhen. Application of rare-earth element Y in refining impure copper. *International Journal of Minerals, Metallurgy, and Materials*, 2015, vol. 22, no. 5, pp. 453–459. DOI: 10.1007/s12613-015-1093-z.
10. Duisemaliev T.U., Duisemaliev U.K. Solubility of yttrium in copper and its effect on the properties of leaded brasses. *Metal Science and Heat Treatment*, 1993, vol. 35, no. 12, pp. 673–676. DOI: 10.1007/BF00707636.
11. Okamoto H. Cu-Y (Copper-Yttrium). *Journal of Phase Equilibria*, 1992, vol. 13, no. 1, pp. 102–103. DOI: 10.1007/BF02645393.
12. Liang Dong, Wang Ning, Wang Yuxiang, Liu Zhenjie, Fu Ying. Effects of Zr, Y on the Microstructure and Properties of As-Cast Cu-0.5Y-xZr (wt.%) Alloys. *Metals*, 2019, vol. 9, no. 10, article number 1084. DOI: 10.3390/met9101084.
13. Zel'dovich V.I., Frolova N.Y., Khomskaya I.V., Kheifets A.E., Dobatkin S.V., Shorokhov E.V., Nasonov P.A. Mechanical properties and the structure of chromium–zirconium bronze after dynamic channel-angular pressing and subsequent aging. *Physics of Metals and Metallography*, 2016, vol. 117, no. 1, pp. 74–82. DOI: 10.1134/S0031918X16010129.
14. Chakrabarti D.J., Laughlin D.E. The Cr-Cu (Chromium-Copper) system. *Bulletin of Alloy Phase Diagrams*, 1984, vol. 5, no. 1, pp. 59–68. DOI: 10.1007/BF02868727.
15. Fonda R.W., Knipling K.E. Texture development in friction stir welds. *Science and Technology of Welding and Joining*, 2011, vol. 16, no. 4, pp. 288–294. DOI: 10.1179/1362171811Y.0000000010.
16. Mishin V., Shishov I., Kalinenko A., Vysotskii I., Zuiko I., Malopheyev S., Mironov S., Kaibyshev R. Numerical Simulation of the Thermo-Mechanical Behavior of 6061 Aluminum Alloy during Friction-Stir Welding. *Journal of Manufacturing and Materials Processing*, 2022, vol. 6, no. 4, article number 68. DOI: 10.3390/jmmp6040068.
17. Arias D., Abriata J.P. Cu-Zr (Copper-Zirconium). *Journal of Phase Equilibria*, 1990, vol. 11, no. 5, pp. 452–459. DOI: 10.1007/BF02898260.
18. Bourezg Y.I., Abib K., Azzeddine H., Bradai D. Kinetics of Cr clustering in a Cu-Cr-Zr alloy processed by equal-channel angular pressing: A DSC study. *Thermochimica Acta*, 2020, vol. 686, article number 178550. DOI: 10.1016/j.tca.2020.178550.
19. Dölling J., Kracun S.F., Prahl U., Fehlbier M., Zilly A. A Comparative Differential Scanning Calorimetry Study of Precipitation Hardenable Copper-Based Alloys with Optimized Strength and High Conductivity. *Metals*, 2023, vol. 13, no. 1, article number 150. DOI: 10.3390/met13010150.
20. Venghaus H., Chiumenti M., Baiges J., Juhre D., Dialami N. Embedded technology for enhanced modeling of Friction Stir Welding processes. *Computer Methods in Applied Mechanics and Engineering*, 2025, vol. 435, article number 117539. DOI: 10.1016/j.cma.2024.117539.

СПИСОК ЛИТЕРАТУРЫ

1. Макаров А.В., Лежнин Н.В., Котельников А.Б., Вопнерук А.А., Коробов Ю.С., Валиуллин А.И., Волкова Е.Г. Восстановление стенок кристаллизаторов машин непрерывного литья заготовок из хромоциркониевой бронзы методом многопроходной сварки трением с перемешиванием // Известия высших учебных заведений. Цветная металлургия. 2023. Т. 29. № 6. С. 66–83. DOI: 10.17073/0021-3438-2023-6-66-83.
2. Bodyakova A.I., Chistyukhina E.I., Tkachev M.S., Malofeev S.S., Kaibyshev R.O. Effect of Friction Stir Processing on the Structure and Properties of the Low-Doped Cu–Cr–Zr Alloy // Physics of Metals and Metallography. 2024. Vol. 125. № 11. P. 1192–1200. DOI: 10.1134/S0031918X24601677.
3. Bodyakova A., Malopfeev S., Tkachev M., Chistyukhina E., Mironov S., Lezhnin N., Fu Y., Makarov A., Kaibyshev R. Effect of friction-stir processing and subsequent aging treatment on microstructure and service properties of Cu-Cr-Zr alloy // Materials Characterization. 2024. Vol. 216. Article number 114225. DOI: 10.1016/j.matchar.2024.114225.
4. Wang Y.D., Liu M., Yu B.H., Wu L.H., Xue P., Ni D.R., Ma Z.Y. Enhanced combination of mechanical properties and electrical conductivity of a hard state Cu-Cr-Zr alloy via one-step friction stir processing // Journal of Materials Processing Technology. 2021. Vol. 288. Article number 116880. DOI: 10.1016/j.jmatprotec.2020.116880.
5. Khomskaya I.V., Zel'dovich V.I., Frolova N.Y., Abdullina D.N., Kheifets A.E. Investigation of Cu_5Zr particles precipitation in Cu-Zr and Cu-Cr-Zr alloys subjected to quenching and high strain rate deformation // Letters on Materials. 2019. Vol. 9. № 4. P. 400–404. DOI: 10.22226/2410-3535-2019-4-400-404.
6. Ma Yuxia, Chen Huiqin, Li Hui, Dang Shue. Influence Mechanism of Ageing Parameters of Cu-Cr-Zr Alloy on Its

Structure and Properties // Materials. 2022. Vol. 15. № 21. Article number 7605. DOI: 10.3390/ma15217605.
7. Khomskaya I.V., Zel’dovich V.I., Abdullina D.N., Shorokhov E.V. The Effect of Chromium and Zirconium Alloying on the Structure and Properties of Submicrocrystalline Copper Alloys Obtained by Dynamic Channel-Angular Pressing // Physics of Metals and Metallography. 2024. Vol. 125. № 10. P. 1156–1165. DOI: 10.1134/s0031918x24601434.
8. Li Yijun, Zhang Jinghua, Fu Ruidong, Wang Jungao, Lv Hongyan, Xing Haizhi. Synergistic improvement of strength and electrical conductivity in Cu–Cr–Zr alloys through prestrain-assisted friction stir processing // Journal of Materials Research and Technology. 2023. Vol. 27. P. 564–573. DOI: 10.1016/j.jmrt.2023.09.262.
9. Li Hai-hong, Sun Xue-qin, Zhang Shang-zhou, Zhao Qin-yi, Wang Guang-zhen. Application of rare-earth element Y in refining impure copper // International Journal of Minerals, Metallurgy, and Materials. 2015. Vol. 22. № 5. P. 453–459. DOI: 10.1007/s12613-015-1093-z.
10. Duisemaliev T.U., Duisemaliev U.K. Solubility of yttrium in copper and its effect on the properties of leaded brasses // Metal Science and Heat Treatment. 1993. Vol. 35. № 12. P. 673–676. DOI: 10.1007/BF00707636.
11. Okamoto H. Cu-Y (Copper-Yttrium) // Journal of Phase Equilibria. 1992. Vol. 13. № 1. P. 102–103. DOI: 10.1007/BF02645393.
12. Liang Dong, Wang Ning, Wang Yuxiang, Liu Zhenjie, Fu Ying. Effects of Zr, Y on the Microstructure and Properties of As-Cast Cu-0.5Y-xZr (wt.%) Alloys // Metals. 2019. Vol. 9. № 10. Article number 1084. DOI: 10.3390/met9101084.
13. Зельдович В.И., Добаткин С.В., Фролова Н.Ю., Хомская И.В., Хейфец А.Э., Шорохов Е.В., Насонов П.А. Механические свойства и структура хромоциркониевой бронзы после динамического канально-углового прессования и последующего старения // Физика металлов и металловедение. 2016. Т. 117. № 1. С. 79–87. DOI: 10.7868/S0015323016010125.
14. Chakrabarti D.J., Laughlin D.E. The Cr-Cu (Chromium-Copper) system // Bulletin of Alloy Phase Diagrams. 1984. Vol. 5. № 1. P. 59–68. DOI: 10.1007/BF02868727.
15. Fonda R.W., Knipling K.E. Texture development in friction stir welds // Science and Technology of Welding and Joining. 2011. Vol. 16. № 4. P. 288–294. DOI: 10.1179/1362171811Y.0000000010.
16. Mishin V., Shishov I., Kalinenko A., Vysotskii I., Zuiko I., Malopheyev S., Mironov S., Kaibyshev R. Numerical Simulation of the Thermo-Mechanical Behavior of 6061 Aluminum Alloy during Friction-Stir Welding // Journal of Manufacturing and Materials Processing. 2022. Vol. 6. № 4. Article number 68. DOI: 10.3390/jmmp6040068.
17. Arias D., Abriata J.P. Cu-Zr (Copper-Zirconium) // Journal of Phase Equilibria. 1990. Vol. 11. № 5. P. 452–459. DOI: 10.1007/BF02898260.
18. Bourezg Y.I., Abib K., Azzeddine H., Bradai D. Kinetics of Cr clustering in a Cu-Cr-Zr alloy processed by equal-channel angular pressing: A DSC study // Thermochimica Acta. 2020. Vol. 686. Article number 178550. DOI: 10.1016/j.tca.2020.178550.
19. Dölling J., Kracun S.F., Prahl U., Fehlbier M., Zilly A. A Comparative Differential Scanning Calorimetry Study of Precipitation Hardenable Copper-Based Alloys with Optimized Strength and High Conductivity // Metals. 2023. Vol. 13. № 1. Article number 150. DOI: 10.3390/met13010150.
20. Venghaus H., Chiumenti M., Baiges J., Juhre D., Dialami N. Embedded technology for enhanced modeling of Friction Stir Welding processes // Computer Methods in Applied Mechanics and Engineering. 2025. Vol. 435. Article number 117539. DOI: 10.1016/j.cma.2024.117539.

УДК 691.73
doi: 10.18323/2782-4039-2025-3-73-5

Особенности формирования микроструктуры в Cu–Cr–Zr–Y бронзе в условиях низкотемпературной обработки трением с перемешиванием

Никитин Иван Сергеевич*[1], кандидат технических наук, младший научный сотрудник лаборатории механических свойств наноструктурных и жаропрочных материалов
Калиненко Александр Андреевич[2], кандидат физико-математических наук, младший научный сотрудник лаборатории механических свойств наноструктурных и жаропрочных материалов
Малофеев Сергей Сергеевич[3], кандидат технических наук, старший научный сотрудник лаборатории механических свойств наноструктурных и жаропрочных материалов
Миронов Сергей Юрьевич[4], доктор физико-математических наук, ведущий научный сотрудник лаборатории механических свойств наноструктурных и жаропрочных материалов
Бодякова Анна Игоревна[5], кандидат физико-математических наук, научный сотрудник лаборатории механических свойств наноструктурных и жаропрочных материалов
Белгородский государственный национальный исследовательский университет, Белгород (Россия)

***E-mail:** nikitin_i@bsuedu.ru

[1]ORCID: https://orcid.org/0000-0002-5417-9857
[2]ORCID: https://orcid.org/0000-0001-7534-0542
[3]ORCID: https://orcid.org/0000-0001-9145-3723
[4]ORCID: https://orcid.org/0000-0003-2202-1518
[5]ORCID: https://orcid.org/0000-0002-9378-0338

Поступила в редакцию 15.07.2025 *Пересмотрена 26.08.2025* *Принята к публикации 09.09.2025*

Аннотация: Применение обработки трением с перемешиванием (ОТП) для модификации физических и механических свойств термически упрочняемых низколегированных бронз является перспективной и одновременно сложной задачей по причине широкого температурного интервала его осуществления. Сложность в том, что в результате ОТП бронз могут формироваться кардинально разные типы микроструктур с широким диапазоном размеров зерен и различным сочетанием типов упрочняющих фаз и их разнообразных морфологий. Более того, возможны варианты, при которых ОТП приводит к деградации свойств бронз. Благоприятное сочетание свойств может быть достигнуто в результате осуществления низкотемпературной ОТП. В рамках работы проведен анализ основных микроструктурных изменений перспективной Cu–Cr–Zr–Y бронзы при ОТП со скоростью вращения инструмента 1000 об/мин и скоростью подачи 25 мм/мин (обеспечивающих температуру в зоне перемешивания ≈350 °C) – низкотемпературной ОТП. Методами растровой электронной микроскопии и EBSD-анализа выявлены механизмы формирования ультрамелкозернистой структуры с преимущественно большеугловыми границами, а также развитие двух типов кристаллографических текстур простого сдвига. Показано, что фаза Cu_x(Y,Zr), наблюдающаяся в исходной структуре, может претерпевать механическое разрушение или же сохранять геометрические параметры в зависимости от своей исходной морфологии и расположения. Впервые показано, что избыточные частицы Cr (равновесная доля при температуре нагрева под закалку) могут не разрушаться, а пластически деформироваться с сильным изменением своей морфологии. При ОТП исследуемой бронзы происходит выделение частиц новой Y-содержащей фазы. Рассмотрена взаимосвязь распределения микротвердости и электропроводности с наблюдаемыми изменениями микроструктуры в новом перспективном материале.

Ключевые слова: обработка трением с перемешиванием; низколегированные бронзы; рекристаллизация; вторичные фазы; электропроводность.

Благодарности: Исследование выполнено за счет гранта Российского научного фонда № 24-29-00628 (https://rscf.ru/project/24-29-00628/) с использованием оборудования Центра коллективного пользования «Технологии и Материалы НИУ "БелГУ"».

Статья подготовлена по материалам докладов участников XII Международной школы «Физическое материаловедение» (ШФМ-2025), Тольятти, 15–19 сентября 2025 года.

Для цитирования: Никитин И.С., Калиненко А.А., Малофеев С.С., Миронов С.Ю., Бодякова А.И. Особенности формирования микроструктуры в Cu–Cr–Zr–Y бронзе в условиях низкотемпературной обработки трением с перемешиванием // Frontier Materials & Technologies. 2025. № 3. С. 67–80. DOI: 10.18323/2782-4039-2025-3-73-5.